ISSN 1674-1056
http://cpb.iphy.ac.cn
http://iopscience.iop.org/cpb
中国物理 B
Chinese Physics
Chinese Physics B

An improved secondary electrons energy spectrum model and its application in multipactor discharge

Wan-Zhao Cui(崔万照), Heng Zhang(张恒), Yun Li(李韵), Yun He(何鋆), Qi Wang(王琪), Hong-Tai Zhang(张洪太), Hong-Guang Wang(王洪广), Jing Yang(杨晶)
Citation: Chin. Phys. B . 2018, 27(3): 038401. **doi:** 10.1088/1674-1056/27/3/038401

Journal homepage: http://cpb.iphy.ac.cn; http://iopscience.iop.org/cpb

What follows is a list of articles you may be interested in

The coupling effect of air-bridges on broadband spiral inductors in SiC-based MMIC technology

Jia-Xin Zheng(郑佳欣), Xiao-Hua Ma(马晓华), Yang Lu(卢阳), Bo-Chao Zhao(赵博超), Heng-Shuang Zhang(张恒爽), Meng Zhang(张濛), Li-Xiang Chen(陈丽香), Qing Zhu(朱青), Yue Hao(郝跃)
Chin. Phys. B . 2017, 26(8): 088401. **doi:** 10.1088/1674-1056/26/8/088401

An efficient multipaction suppression method in microwave components for space application

Wan-Zhao Cui(崔万照), Yun Li(李韵), Jing Yang(杨晶), Tian-Cun Hu(胡天存), Xin-Bo Wang(王新波), Rui Wang(王瑞), Na Zhang(张娜), Hong-Tai Zhang(张洪太), Yong-Ning He(贺永宁)
Chin. Phys. B . 2016, 25(6): 068401. **doi:** 10.1088/1674-1056/25/6/068401

Switching mechanism for TiO_2 memristor and quantitative analysis of exponential model parameters

Wang Xiao-Ping, Chen Min, Shen Yi
Chin. Phys. B . 2015, 24(8): 088401. **doi:** 10.1088/1674-1056/24/8/088401

Characteristics of titanium oxide memristor with coexistence of dopant drift and a tunnel barrier

Tian Xiao-Bo, Xu Hui
Chin. Phys. B . 2014, 23(6): 068401. **doi:** 10.1088/1674-1056/23/6/068401

Three-dimensional simulation method of multipactor in microwave components for high-power space application

Li Yun, Cui Wan-Zhao, Zhang Na, Wang Xin-Bo, Wang Hong-Guang, Li Yong-Dong, Zhang Jian-Feng
Chin. Phys. B . 2014, 23(4): 048402. **doi:** 10.1088/1674-1056/23/4/048402

An improved secondary electrons energy spectrum model and its application in multipactor discharge*

Wan-Zhao Cui(崔万照)[1,†], Heng Zhang(张恒)[1], Yun Li(李韵)[1], Yun He(何鋆)[1], Qi Wang(王琪)[1], Hong-Tai Zhang(张洪太)[1], Hong-Guang Wang(王洪广)[2], and Jing Yang(杨晶)[1]

[1] National Key Laboratory of Science and Technology on Space Microwave, China Academy of Space Technology (Xi'an), Xi'an 710100, China
[2] School of Electronic and Information Engineering, Xi'an Jiaotong University, Xi'an 710049, China

(Received 3 September 2017; revised manuscript received 7 December 2017; published online 11 February 2018)

Secondary electron emission (SEE) of metal and dielectric materials plays a key role in multipactor discharge, which is a bottle neck problem for high-power satelliate components. Measurements of both the secondary electron yield (SEY) and the secondary electron energy spectrum (SES) are performed on metal samples for an accurate description of the real SEE phenomenon. In order to simplify the fitting process and improve the simulation efficiency, an improved model is proposed for the description of secondary electrons (SE) emitted from the material surface, including true, elastic, and inelastic SE. Embedding the novel SES model into the electromagnetic particle-in-cell method, the electronic resonant multipactor in microwave components is simulated successfully and hence the discharge threshold is predicted. Simulation results of the SES variation in the improved model demonstrate that the multipactor threshold is strongly dependent on SES. In addition, the mutipactor simulation results agree quite well with the experiment for the practical microwave component, while the numerical model of SEY and SES fits well with the sample data taken from the microwave component.

Keywords: secondary electron energy spectrum, multipactor simulation, vaccum breakdown, satellite application

PACS: 84.32.–y, 52.40.Db, 79.20.Ap **DOI:** 10.1088/1674-1056/27/3/038401

1. Introduction

Multipactor discharge, known as the resonant secondary electron (SE) avalanche effect, is a phenomenon caused by secondary electron emission (SEE) and its synchronism with electromagnetic wave.[1–3] In recent years, with the wide spread application of high power microwave components in the space-industry, multipactor issues have become a huge potential risk.[4–8] When it occurs, accelerated electrons deposit considerable energy on a tiny spot, leading to power dissipation, electrical performance degradation, surface damage, and even irreversible device destruction.[6,9,10]

Multipactor discharge depends on many factors, among which the most important one is the SEE property of the material. The secondary electron yield (SEY) and secondary electron spectrum (SES) are commonly used to characterize the SEE properties of materials. SEY significantly affects the multipactor threshold.[11–16] Vaughan's formulism was based on a semi-empirical equation fitted to the total secondary electron yield for a given material.[1,17,18] Furman and Pivi gave a model that distinguished different physical mechanisms and probabilities of secondary electron emission, including inelastic and elastic scatterings.[18,19] However, there were many unphysical parameters in the Furman model, which made exact fitting very difficult. Chung and Everhart presented a simple calculation of the energy distribution of low-energy secondary electrons.[20] The normalized model was brief, containing no free parameters, and had a good fit to experimental data in its low-energy end. However, this model only described the true-secondary electron of SEE. In addition, the accurate full wave simulation investigation means of multipactor and the quantitative relationship between SES and multipactor are still lacking.[21–25] In this paper, an improved numerical model is proposed. This model mainly describes the energy spectrum distribution of the secondary electrons emitted from the metal material surface, including true, elastic, and inelastic secondaries. In addition, based on the SES measurements and multipactor simulation software MSAT,[13,14] the numerical relationship between SES and multipactor threshold is established. Effects of the SES on multipactor analysis of microwave components are investigated numerically and experimentally. The results of simulation and experiment indicate that the threshold prediction accuracy reached 0.3 dB in multipactor simulation, while the improved SES model fitting accuracy reaches 99%.

2. The improved SES model

SEE phenomenon is described by two main parameters SEY and SES. For a steady monoenergetic electron beam impinging on a metal surface, SEY is defined by $\delta = N_s/N_0$,

*Project supported by the National Natural Science Foundation of China (Grant Nos. U1537211, 11705142, and 11675278) and the National Key Laboratory Foundation, China (Grant No. 9140C530101150C53011).

†Corresponding author. E-mail: cuiwanzhao@126.com

© 2018 Chinese Physical Society and IOP Publishing Ltd

where N_0 is the incident electrons number and N_s is the number of the produced secondary electrons. However, for the SEY measurement, it is defined by $\delta = I_s/I_0$, where I_0 is the incident electron beam current and I_s is the collected secondary electron current, i.e., the electron current emitted from the sample surface. The SES is defined to be

$$f(E) = \frac{\mathrm{d}\delta}{\mathrm{d}E}. \tag{1}$$

For the physical convergence, the energy integral of SES is equal to the yield at certain incident energy, which is called the normalization condition,

$$\int_0^{E_0} f(E)\mathrm{d}E = \delta(E_0). \tag{2}$$

When a steady current I_0 of electrons impinges on a metal surface, part of I_e is reflected elastically while the rest penetrates into the material. Some of the incident electrons scatter from one or more atoms inside the metal and the scattered electrons are reflected back out. These are the so-called rediffused electrons and the corresponding current is I_r. The rest of the incident electrons interact with the metal in a more complicated way and yield the true secondary electrons (TSE) and the corresponding current I_{ts}. The yields of each type are defined by $\delta_e = I_e/I_0$, $\delta_r = I_r/I_0$, and $\delta_{ts} = I_{ts}/I_0$. In correspondence with the SEYs, the SES of each type are defined by $f_e = \mathrm{d}\delta_e/\mathrm{d}E$, $f_r = \mathrm{d}\delta_r/\mathrm{d}E$, and $f_{ts} = \mathrm{d}\delta_{ts}/\mathrm{d}E$, which also satisfy the normalization condition. Thus, the total SES is

$$\frac{\mathrm{d}\delta}{\mathrm{d}E} = f_e + f_r + f_{ts}. \tag{3}$$

However, the distinction between these three types of electrons is equivocal in the macroscopic view. Then, in the simulation and experiment investigation, the secondary electrons are divided according to their energy ranges, as shown in Fig. 1.[26]

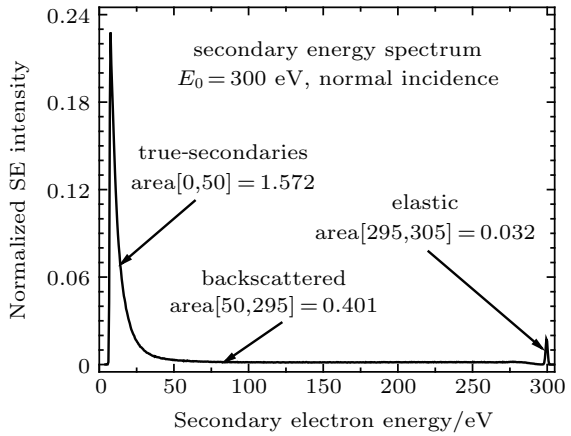


Fig. 1. Measured SES of silver-coating at $E_0 = 300$ eV for normal incidence. Three characteristic SEYs are given by integration on the corresponding energy ranges of SES (area $[E_1, E_2]$). Thus for this case, $\delta_{ts} = 1.572$, $\delta_r = 0.401$, and $\delta_e = 0.032$. The upper energy cutoff for the true secondaries is somewhat arbitrarily, but conventionally, chosen to be 50 eV.

According to the figure configuration in the high-energy end, the distribution function for the elastic electrons is given by

$$f_e(E) = \delta_e(E_0, \theta_0) \frac{2\exp\left[-(E-E_0)^2/2\sigma_e^2\right]}{\sqrt{2\pi}\sigma_e \mathrm{erf}\left(E_0/\sqrt{2}\sigma_e\right)}, \tag{4}$$

which is normalized so that it satisfies

$$\int_0^{E_0} f_e(E)\mathrm{d}E = \delta_e(E_0, \theta_0), \tag{5}$$

where E_0 and θ_0 are the incident electron energy and angle, E is the emitted electron energy, and σ_e is a fitting parameter for the elastic SES.

Similarly, the SES for the rediffused electrons is given by

$$f_r(E) = \delta_r(E_0, \theta_0) \frac{(q+1)}{E_0} \left(\frac{E}{E_0}\right)^q, \tag{6}$$

which satisfies the normalization condition

$$\int_0^{E_0} f_r(E)\mathrm{d}E = \delta_r(E_0, \theta_0), \tag{7}$$

where q is a fitting parameter for the rediffused SES.

Consider an energetic primary electron impinging on a semi-infinite metal plate in a vacuum. The incident primary direction is denoted as the z axis. We only consider the case of normal incidence, and assume that the secondary electron excitation process is isotropic. That is, all directions of motion of an excited internal secondary electron are equally probable. We assume that any scattering of an excited secondary electron with the electron gas in the solid produces absorption, hence only electrons that are not scattered between their point of excitation and the surface can escape. This assumption is believed to be correct for low-energy excited electrons as the energy loss involved in a scattering with the electron gas is appreciable. When the energy of the excited electron increases, the assumption becomes more approximate. As we use a degenerate free-electron-gas model for the solid, collisions with the ions and other band-structure-related effects are automatically precluded. We have

$$\frac{\mathrm{d}N}{\mathrm{d}E'} = \frac{S(E')\lambda(E')}{2} \int_0^{\theta_m} \sin\theta\cos\theta\,\mathrm{d}\theta, \tag{8}$$

with

$$S(E') = \frac{e^4 k_F^3}{3\pi E_p (E' - E_F)^2}, \tag{9}$$

$$\lambda(E') = \frac{14.7(E_F\beta)^{3/2} E'(E'-E_F)^{-2}}{(m^*)^{1/2}\left[\tan^{-1}(1/\beta)^{1/2} + \beta^{1/2}/(1+\beta)\right]}, \tag{10}$$

where θ_m is defined as the maximum allowed value of θ for escape. The function $S(E')$ has been calculated by Streitwolf and also earlier by Baroody. For $\lambda(E')$, we use Quinn's result as given in Kanter's paper.

From Eqs. (8)–(10) we can obtain the simplified expression of $\mathrm{d}N/\mathrm{d}E'$

$$\frac{\mathrm{d}N}{\mathrm{d}E'} = k\frac{(E'-E_\mathrm{F}-\Phi)}{(E'-E_\mathrm{F})^4}, \tag{11}$$

where k is a constant, which is dependent on the material characteristics. From Eq. (11), we see that the shape of $\mathrm{d}N/\mathrm{d}E'$ is entirely determined by the factor $f(E') = (E'-E_\mathrm{F}-\Phi)/(E'-E_\mathrm{F})^4$. We find that E' is the energy of the excited secondary electron. In order to fit the measurement data, we should convert E' into E, the energy of the secondary electron at the metal-vacuum interface, $E = E'-\Phi-E_\mathrm{F}$. Then, we can obtain the converted factor $f(E') = E/(E+\Phi)^4$. The simplified expression of $\mathrm{d}N/\mathrm{d}E$ is

$$\frac{\mathrm{d}N}{\mathrm{d}E} = k\frac{E}{(E+\Phi)^4}. \tag{12}$$

Using the regular pattern of the elastic and re-diffused electrons model, we can obtain the most important part, the true secondary electron spectrum as

$$\begin{aligned} f_\mathrm{ts}(E) &= \delta_\mathrm{ts}(E_0,\theta_0)\frac{E}{(E+\Phi)^4\int_0^{E_0}\frac{E}{(E+\Phi)^4}\mathrm{d}E} \\ &= \delta_\mathrm{ts}(E_0,\theta_0)\frac{6\Phi^2(E_0+\Phi)^3E}{E_0^2(E_0+3\Phi)(E+\Phi)^4}, \end{aligned} \tag{13}$$

which also satisfies the normalization condition

$$\int_0^{E_0} f_\mathrm{ts}(E)\mathrm{d}E = \delta_\mathrm{ts}(E_0,\theta_0), \tag{14}$$

where Φ is defined as the work function of the metal surface and is adjustable in multipactor simulation investigation. In this model, the distribution probability of the true secondary electrons is described by the polynomial and fitted mainly by the parameter of the surface work function, which is not only of high efficiency but also simple in expression and convenient to embed in multipactor numerical simulation.

3. Simulation investigation of SES on multipactor

3.1. Quantitative relationship between SES and multipactor threshold

In the literature, the secondary energy spectrum has never been taken into account for multipactor simulation. Difficulties lie not only in the measurement but also on the curve fitting. In our previous work, the simulation method of multipactor, MSAT, was established based on the EM-PIC method.[13–15]

Since the finite-difference time-domain (FDTD) method is adopted for EM field calculaton, the studied object is first discretized into small meshes. Then, the particle-in-cell (PIC) method is used for the calculation of electron dymamics. Macroparticle, rather than the real electrons, is used in the model for numerical simplification.

The three-dimensional multipactor simulation involves the following five main steps: (i) three-dimensional modeling of the component and spatial discretization, (ii) fields and particles initialization, (iii) the field-to-electron and electron-to-field iteration calculation, (iv) secondary electron emission modeling, and (v) multipactor threshold prediction. Then, through electron trajectory tracking and collection, multipactor discharge threshold of the practical component can be analyzed from the transient evolution trend of the secondary electron number or total electron number.

In this paper, by using the established SES models, the emission energy spectrum has been successfully described and embedded in the numerical algorithm of multipactor simulation, as shown in Fig. 2. As shown in Fig. 2, the multipactor simulation is divided into three significant processes: the full-wave simulation of field, the particle-in-cell simulation of electron' motion, and the modeling of SEE, including SEY and SES. Primary particles should be initiated properly to describe the real electron distribution in the space.

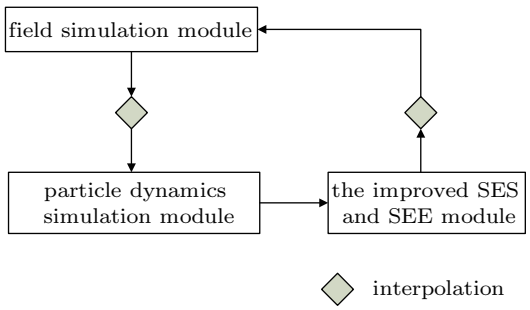


Fig. 2. (color online) Schematic program of multipactor simulation.

3.2. Simulation results

A typical microwave component, the impedance transformer, is selected for the analysis and simulation validation of multipactor. The test frequency is 12 GHz. The three dimensional model and dimensions are shown in Fig. 3.

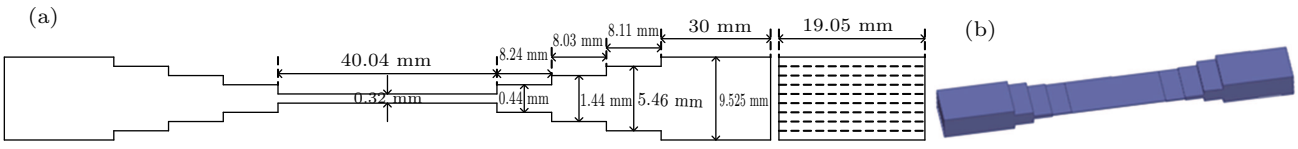


Fig. 3. (color online) Impedance transformer: (a) dimensions, (b) three-dimensional model.

The EM-PIC method with the improved model is utilized to investigate the effect of SES on the multipactor threshold. Multipactor simulations with different SES distributions while keeping the same SEY are performed on the impedance transformer. The low energy end is mainly related to the TSE part. Thus, the parameter scanning investigation of Φ is performed to form different low-energy end distributions.

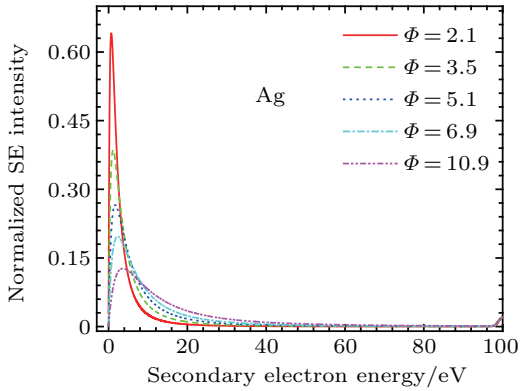


Fig. 4. (color online) Emitted energy spectrum with different Φ.

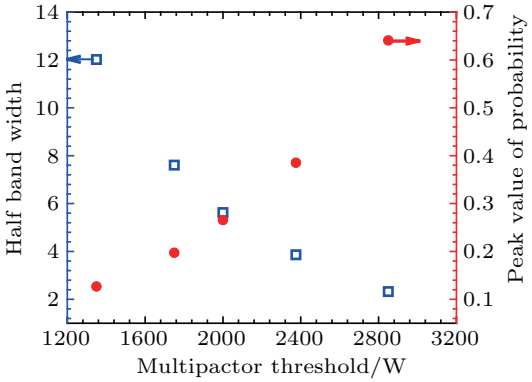


Fig. 5. (color online) Multipactor threshold with different peak values and half peak widths within the low-energy end.

Figures 4 and 5 indicate that the multipactor threshold increases as the peak value of the low-energy end increases, while the half peak width of the low-energy end decreases, simultaneously. And the multipactor threshold is almost in linear proportion to the peak value of SES and varies in inverse proportion to the half peak width of the low-energy end of SES. Therefore, it is conjectured that the multipactor threshold increases when a bigger proportion of secondary electrons lies in the low-energy end where the emission energy ranges from 0 to 50 eV.

In addtion, for this transformer, it is found that when the maximum of the low-energy peak increases from 0.127 to 0.641, the multipactor threshold is elevated by 3.2 dB. When the half peak width decreases from 12.02 to 2.32, the multipactor threshold is elevated by 3.2 dB. It is indicated that the simulation accuracy of the multipactor strongly depends on the accuracy of the SES model and data used in the simulation.

4. SEE experimental results

Figure 6 shows the ultra-high vacuum (UHV) system for SEY and SES measurements of metal. The UHV chamber and the load-lock chamber have ultimate vacuum degrees of 9×10^{-9} Pa and 5×10^{-7} Pa, respectively. The UHV chamber is equipped with a sample stage, a residual gas analyzer (RGA), a sputtering ion gun with argon gas supply for surface cleaning, and an automatic dual-pass energy analyzer with an integral gun for the test of the secondary electron energy spectrum (DESA 150). DESA 150 is a two-stage energy spectrometer. Both stages, including input lens and energy spectrometer, are derived from a cylindrical mirror configuration. The focusing is achieved by adjusting the potential of both the inner and outer cylinders. Particles enter the cylindrical mirror field between the cylinders instead of passing through a slit into the inner cylinder. The advantage is a large working distance between the spectrometer and sample, as long as 55 mm, which can be varied by 3 mm without degrading the signal. The energy of the particles passing though the spectrometer can be adjusted and the energy resolution can be electrically selected over a wide range of values (100 meV up to 6 eV).

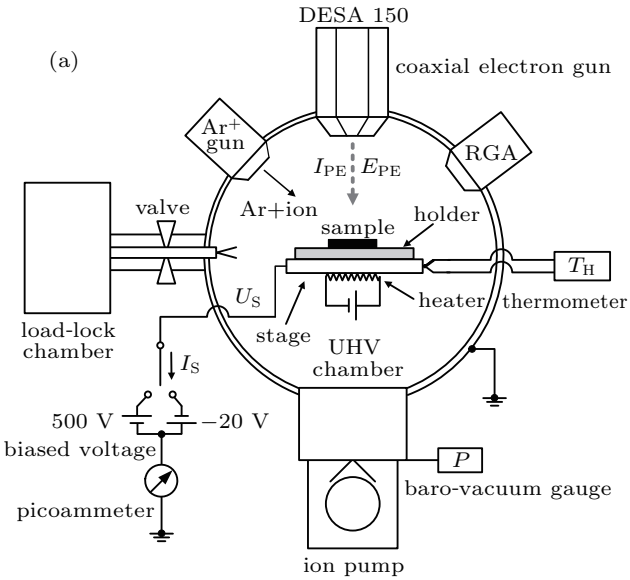




Fig. 6. (color online) (a) The scheme of SEE measurement system, (b) SEE measurement platform.

The SEE properties of the same material may vary to a large extent for different surface states. Consequently, measurement data in the literature are not sufficient to describe the surface SEE of a concrete device in practice, especially for the multipactor threshold simulation. By using the established UHV system, SEE data of samples under the same processing procedure and condition of practical components are measured and fitted by the SES model.

The samples are shaped in a rectangle of 20 mm×15 mm, coated by ∼6 μm silver on a 1 mm thick aluminum alloy base plate. The incident energy probability $\mathrm{d}\delta/\mathrm{d}E$ is measured and calculated at $E_0 = 90$ eV. In addition, to obtain a relatively accurate description of the surface SEE and multipactor simulation results, the SEY model is also fitted. The fitted data and parameters are given in Figs. 7 and 8 and Table 1.

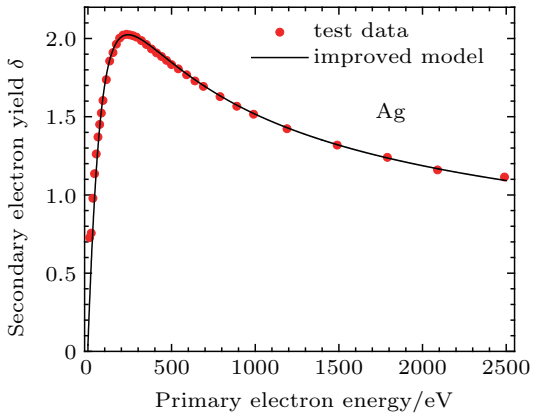


Fig. 7. (color online) The SEY of silver-coated samples.

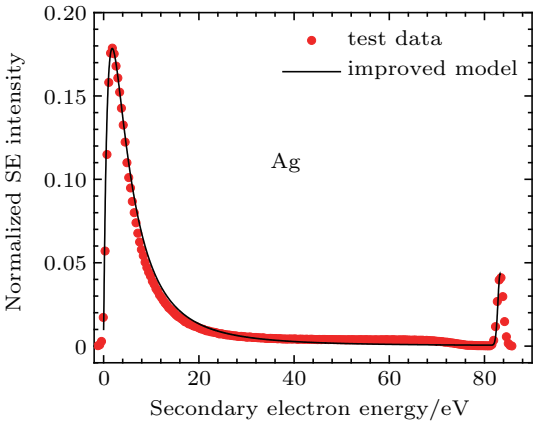


Fig. 8. (color online) The SES of silver-coated samples at 90 eV for normal incidence.

Table 1. Parameters for the fit of the improved SES model of silver-coated samples.

$P_{1,\mathrm{e}}(\infty)$	$P_{1,\mathrm{e\,max}}$	$E_{\mathrm{e\,max}}$	W	p	E_0	σ_{e}	$P_{1,\mathrm{r}}(\infty)$
0.025	0.04	0	20.86	1	83.3	0.47	0.01
E_{r}	r	q	$\delta_{\mathrm{ts\,max}}(0)$	$E_{\mathrm{ts\,max}}(0)$	s	Φ	
0.041	0.104	0.4	1.99	240	1.41	5.5	

Table 1 shows that only three parameters of the improved model are used to fit the experimental SES data, which is of high efficiency and accuracy. The fitted data matches very well with the measured ones. The mean square deviation of measurement error for silver is 0.0123.

By using the established measurement system and the improved SES models, the real emission energy spectrum has been successfully measured and fitted. In our previous work, the EM-PIC simulation method of the multipactor has been established. Embedded in the fitted SES model, multipactor simulation on practical components considering the real SEE description is implemented.

5. Multipactor experimental results

As shown in Fig. 9, the incident-reflected power zeroing method is used for the measurement of multipactor threshold. In the vacuum chamber, after the 3 dB bridge and the variable attenuator, the reflected power from the device under test (DUT) is of the same magnitude but the reversed phase as the coupled incident power. The zeroing single is obtained and detected by the spectrometer. If the multipactor in DUT occurs, the balance state will be broken and a jumping signal is observed on the spectrum analyzer.

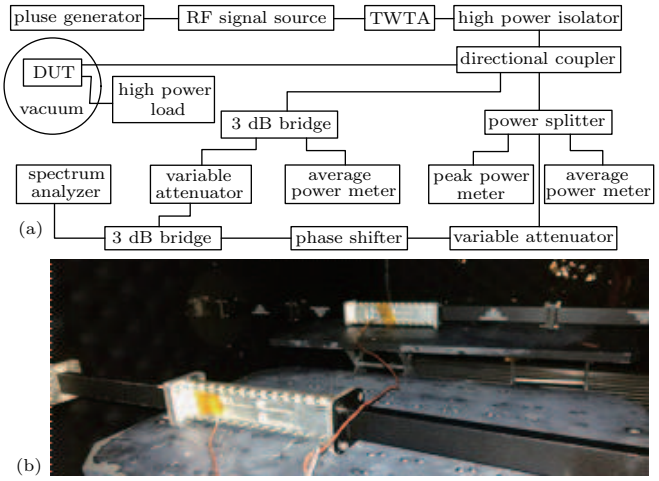


Fig. 9. (color online) Multipactor measurement system: (a) the schematic diagram, (b) platform picture.

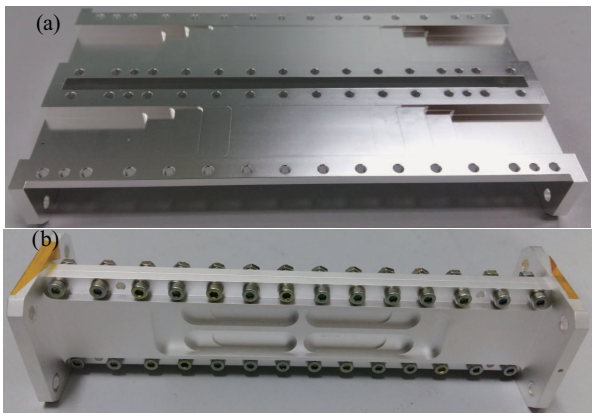


Fig. 10. (color online) Prototypes of the impedance transformer: (a) pieces of the transformer, (b) assembled device.

Figure 10 shows the fabrication pieces of the sliver-coated impedance transformer, the dimensions and model of which are shown in Fig. 2. The transformer is made of aluminum base and plated with 10 μm silver. The average surface roughness is about 0.8 μm. Multipactor measurements are performed on it. Multipactor simulation results with the Furman model, the improved model in the EM-PIC method, and the experimental results are recorded in Table 2. The improved SEE model is fitted with the experiment data of silver. The threshold prediction error of the sliver-coated transformer is 0.3 dB. Compared with the Furman model, the simulation accuracy is improved and the fitting procedure is simplified.

Table 2. Comparison of simulated multipactor thresholds with experiments.

Component	MSAT with Furman model	MSAT with the improved model	Experimental threshold
Silver-coated impedance transformer	1000 W	2100 W	1950 W

6. Conclusion

An improved model is proposed for the description of the emission energy distribution for secondary electrons in multipactor simulation. The emission energy distribution upon certain incident energy is well described and fitted by the improved model. Based on the measured data, the fitted model is utilized to mimic the surface emission state of practical components. The whole energy range of the incident electrons is described with improved accuracy according to the measured data and it is simplified for the utilization in multipactor simulation and suppression. Simulation and experiment results demonstrate that the fitting accuracy of 99% in SES and SEY, and threshold prediction error of 0.3 dB in multipactor simulation are reached, respectively, which is promising for multipactor design in space applications.

References

[1] Vaughan J R M 1988 *IEEE Trans. Electron Dev.* **35** 1172
[2] Kishek R, Lau Y Y, Valfells A, Ang K L and Gilgenbach 1998 *Phys. Plasma* **5** 2120
[3] Yang W J, Li Y D and Liu C L 2013 *Acta Phys. Sin.* **62** 087901 (in Chinese)
[4] Song Q Q, Wang X B, Cui W Z, Wang Z Y and Ran L X 2014 *Acta Phys. Sin.* **63** 220205 (in Chinese)
[5] Zhu F, Proch D and Hao J K 2005 *Chin. Phys.* **14** 0494 (in Chinese)
[6] Rozario N and Lenzing H 1994 *IEEE Trans. MTT.* **42** 558
[7] Kudsia C, Cameron R and Tang W C 1992 *IEEE Trans. Microwave Theor. Techniq.* **40** 1133
[8] Li Y D, Yan Y J, Lin S, Wang H G and Liu C L 2014 *Acta Phys. Sin.* **63** 047902 (in Chinese)
[9] Lu Q L, Zhou Z Y, Shi L Q and Zhao G Q 2005 *Chin. Phys.* **14** 1465
[10] Woode A and Petit J 1990 *ESA Journal-European Space Agency* **14** 467
[11] Kossyi I A, Luk'yanchikov G S, Semenov V E, Zharova N A, Anderson D, Lisak M and Puech J 2010 *J. Phys. D: Appl. Phys.* **43** 345206
[12] Zhang N, Cao M, Cui W Z, Hu T C, Wang R and Li Y 2015 *Acta Phys. Sin.* **64** 207901 (in Chinese)
[13] Li Y, Cui W Z, Zhang N, Wang X B, Wang H G, Li Y D and Zhang J F 2014 *Chin. Phys. B* **23** 048402
[14] Li Y, Cui W Z and Wang H G 2015 *Phys. Plasma.* **22** 053108
[15] Li Y and Cui W Z 2012 *Proc. 42nd European Microwave Conference*, 29 October 2012 Amsterdam The Netherlands 920
[16] Cui W Z, Li Y, Yang J, Hu T C, Wang X B, Wang R, Zhang N, Zhang H T and He Y N 2016 *Chin. Phys. B* **25** 068401
[17] Vaughan J R M 1989 *IEEE Trans. Electron Dev.* **36** 1963
[18] Li Y D, Yang W J, Zhang N, Cui W Z and Liu C L 2013 *Acta Phys. Sin.* **62** 077901 (in Chinese)
[19] Furman M A and PiVi M T F 2002 *Phys. Rev. Spec. Top. Accel. Beams.* **5** 124404
[20] Chung M S and Everhart T E 1974 *J. Appl. Phys.* **45** 707
[21] Hockney R W and Eastwood J W 1981 *Computer Simulation Using Particles* (New York: McGraw-Hill)
[22] Eastwood J W 1991 *Comput. Phys. Commun.* **64** 252
[23] Goplen B, Ludeking L, Smithe D and Warren G 1995 *Comput. Phys. Commun.* **87** 54
[24] Liu G Z and Shao H 2003 *Chin. Phys.* **12** 0204
[25] Liu L, Li Y D, Wang R, Cui W Z and Liu C L 2013 *Acta Phys. Sin.* **62** 025201 (in Chinese)
[26] Yang J, Cui W Z, Li Y, Xie G B, Zhang N, Wang R, Hu T C and Zhang H T 2016 *Appl. Surf. Sci.* **382** 88